JOURNAL OF MAGNETIC RESONANCE **132,** 25–33 (1998)
ARTICLE NO. MN981374

3D Accordion Spectroscopy for Measuring ^{15}N and ^{13}CO Relaxation Rates in Poorly Resolved NMR Spectra

Peter A. Carr, David A. Fearing, and Arthur G. Palmer, III[1]

Department of Biochemistry and Molecular Biophysics, Columbia University, 630 West 168th Street, New York, New York 10032

Received September 24, 1997

An experimental approach for the measurement of nuclear magnetic spin relaxation rate constants that combines triple-resonance techniques and accordion spectroscopy is described. Pulse sequences are discussed for the measurement of backbone ^{15}N and ^{13}CO R_1 relaxation rate constants. The three-dimensional HNCO triple-resonance technique is employed to gain improved spectral resolution over conventional two-dimensional methods by frequency labeling both the ^{15}N and ^{13}CO spins. Accordion spectroscopy is used to reduce the dimensionality of the relaxation experiment. The ''negative-time accordion'' approach (A. M. Mandel and A. G. Palmer (1994), *J. Magn. Reson. A* **110, 62–72) is used for extracting rate constants from the t_1 interferograms. The experiments are demonstrated using a ^{13}C/^{15}N isotopically enriched sample of the third fibronectin type III domain of human tenascin.**

Key Words: **NMR; accordion spectroscopy; relaxation.**

INTRODUCTION

Characterization of the dynamical behavior of macromolecules by solution NMR spectroscopy relies on the measurement of nuclear magnetic spin relaxation rate constants (*1*). In the usual approach, a series of 2D heterocorrelation spectra are recorded with different values of a parametric relaxation delay to generate relaxation decay curves. Overlap between resonances in the 2D spectra, particularly for large proteins or molecules with poor resonance dispersion, poses a practical difficulty in these experiments. Spectral resolution enhancement techniques (*2*) or peak deconvolution methods (*3*) can be used to resolve partially overlapped resonances and increase the accuracy of the relaxation rate constants, although usually at a cost of reduced precision. Relaxation decay curves for overlapping resonances also can be fit to more than one decaying exponential function to obtain rate constants for individual signal components; however, poor results are obtained for rate constants close in value (*4*). Despite these approaches, in many cases, a single approximate rate constant must be assigned to a set of overlapped resonances (*5*), or overlapped resonances must be excluded from the study (*6*). In recent years a variety of three- and four-dimensional triple-resonance schemes have been applied in solution NMR spectroscopy for the resolution of overlapping resonances (*7*). These methods can be applied to measurements of relaxation rates by extending the usual series of 2D spectra to a series of 3D spectra; however, this simple approach is not usually practical because the experimental acquisition time is dramatically increased.

Accordion spectroscopy allows the convolution of an indirect evolution dimension of an NMR experiment with an additional time-dependent parameter of interest, and has been used in measurements of chemical exchange (*8, 9*), scalar coupling constants (*10*), TOCSY transfer functions (*11*), and relaxation rate constants (*12, 13*). Accordion spectroscopy is closely related to simultaneous evolution techniques for reducing the dimensionality of triple-resonance NMR experiments (*14*).

Here we demonstrate that accordion spectroscopy and triple-resonance methods can be combined to provide accurate measurements of relaxation rate constants and enhanced spectral resolution of three separate frequency evolution periods. Examples are given for the measurement of ^{15}N and ^{13}CO R_1 relaxation rates in a doubly ^{15}N/^{13}C-labeled sample of the third type III fibronectin domain of human tenascin-C (TNfn3). In these cases, pulse sequences conceptually similar to the HNCO experiment (*15*) and the ^{13}CO spin–lattice relaxation experiment (*16, 17*) have been adapted to include accordion relaxation periods.

THEORY

Accordion spectroscopy combines two time-dependent functions in the same indirect evolution dimension of an NMR experiment by simultaneously covarying two different incrementable time delays. In the case of relaxation measurements, the parametric relaxation delay, T_r, is covaried with the frequency labeling period of an indirectly detected nucleus, such as ^{15}N.

[1] To whom correspondence should be addressed. Fax: (212) 305-7932. E-mail: agp6@columbia.edu.

1090-7807/98 $25.00

For the measurement of spin–lattice relaxation, the time dependence of the signal can be expressed as

$$I(T_r) = I_0 e^{-R_1 T_r} \quad [1]$$

in which I_0 is the magnitude of the initial magnetization, R_1 is the spin–lattice relaxation rate constant, and the dependence of the decay on the long-time steady-state magnetization is assumed to be eliminated by appropriate phase cycling during the pulse sequence (*18*). The dependence of the signal during an indirectly detected evolution period (t_1 evolution) is

$$I(t_1) = I_0 e^{(-i\omega t_1 - R^* t_1)}, \quad [2]$$

in which hypercomplex phase cycling (*19*) or sensitivity-enhanced techniques (*20*) have been used to generate t_1 interferograms that represent complex data vectors. Here ω is the Larmor frequency of the indirectly detected nucleus, and R^* represents any relaxation processes occurring during the evolution period. Combining these two equations yields

$$\begin{aligned} I(t_1, T_r) &= I_0 e^{(-i\omega t_1 - R^* t_1)} e^{(-R_1 T_r)} \\ &= I_0 e^{(-i\omega t_1} e^{-R^* t_1 - R_1 T_r)}. \end{aligned} \quad [3]$$

In conventional relaxation measurements, T_r and t_1 are uncorrelated. Several 2D data sets are acquired, differing only in the value of T_r used, in order to define decay curves according to Eq. [1]. In an accordion experiment, T_r is incremented in proportion to the t_1 increment; thus $\Delta T_r = \kappa \Delta t_1$ where the scaling constant, κ, is chosen based on experimental considerations (*vide infra.*) The resulting t_1 interferogram has a decay envelope that depends on both R^* and R_1. Various schemes for subsequently separating R^* and R_1 have been discussed previously (*12*). Of these, the ''negative-time accordion'' method can be used to maximize the number of t_1 points acquired using a constant-time evolution period, and is employed in the experiments discussed here.

The negative-time accordion requires recording the experiment in two parts, referred to as the forward and reverse components. For the forward component, T_r begins at approximately half its maximal value ($T_r^{mid} = n\kappa\Delta t_1$, where n is the number of complex t_1 points acquired for each of the forward and reverse experiments) and is incremented in proportion to t_1 toward its maximum value (T_r^{max}):

$$T_r^{for} = T_r^{mid} + \kappa t_1. \quad [4]$$

For the reverse experiment, T_r begins at half its maximal value and is decremented with t_1 toward its minimum value (T_r^{min}):

$$T_r^{rev} = T_r^{mid} - \kappa t_1. \quad [5]$$

The resultant time dependence of the interferograms is illustrated in Fig. 1A for the separate forward and reverse components.

After acquisition, the order of complex points in the reverse component of the interferogram is reversed and complex conjugation is performed. The forward component is then appended to the reverse component to generate an interferogram that contains $2n$ complex points, as shown in Figs. 1A and 1B. The resulting interferogram depends differently on R^* and R_1; these values can be distinguished by linear prediction and/or least-squares fitting of the time domain. This treatment of the accordion data is analogous to the negative-time data extension used by Zhu and Bax for linear prediction (*21*).

More formally, the forward and reverse components of the interferogram can be expressed with Eqs. [3]–[5] and using $t_1 = k\Delta t_1$ as

$$I_f(k) = I_0 e^{[-(i\omega + R^*)k\Delta t_1 - \kappa R_1 (n+k)\Delta t_1]} \quad [6]$$

$$I_r(k) = I_0 e^{[-(i\omega + R^*)k\Delta t_1 - \kappa R_1 (n-k)\Delta t_1]}, \quad [7]$$

where n is the number of complex points taken for each of the forward and reverse components and k increments from $\frac{1}{2}$ to $n - \frac{1}{2}$. Thus for each component, the initial value of t_1 is set to $\Delta t_1/2$ (*22*), the initial value of $T_r^{for} = (n + \frac{1}{2})\kappa\Delta t_1$, and the initial value of $T_r^{rev} = (n - \frac{1}{2})\kappa\Delta t_1$. Making the substitution $p = -k$ and taking the complex conjugate of Eq. [7] yields

$$I_r(p) = I_0 e^{[-(i\omega - R^*)p\Delta t_1 - \kappa R_1 (n+p)\Delta t_1]} \quad [8]$$

in which p ranges from $-\frac{1}{2}$ to $-(n - \frac{1}{2})$. Equations [6] and [8] can be combined to yield a single data set described by

$$I(k) = I_0 e^{[-i\omega k\Delta t_1 - |k| R^* - \kappa R_1 (n+k)\Delta t_1]}, \quad [9]$$

in which k ranges from $-(n - \frac{1}{2})$ to $(n - \frac{1}{2})$. This equation is representative of the interferogram shown at the top of Fig. 1B. In practice, the desired T_r^{max} is chosen first, usually in the range of $0.7/R_1$ to $2/R_1$, and κ is calculated as $\kappa = T_r^{max}/[(2n - \frac{1}{2})\Delta t_1]$.

Figure 2 shows pulse sequences for the measurement of ^{13}CO R_1 relaxation rates in proteins. The ''conventional'' experiment represented in Fig. 2A is based on that of Zuiderweg and co-workers (*16*), extended to include coherence selection and PEP sensitivity enhancement via pulsed field gradients (*23*). This experiment is intended to be recorded as a series of $^{15}N-^{1}H$ 2D correlation spectra, each varying by the relaxation delay T_r. In contrast, the new experiment introduced in Fig. 2B is used to generate a single 3D data set, with frequency evolution in the t_1 (^{13}CO), t_2 (^{15}N), and

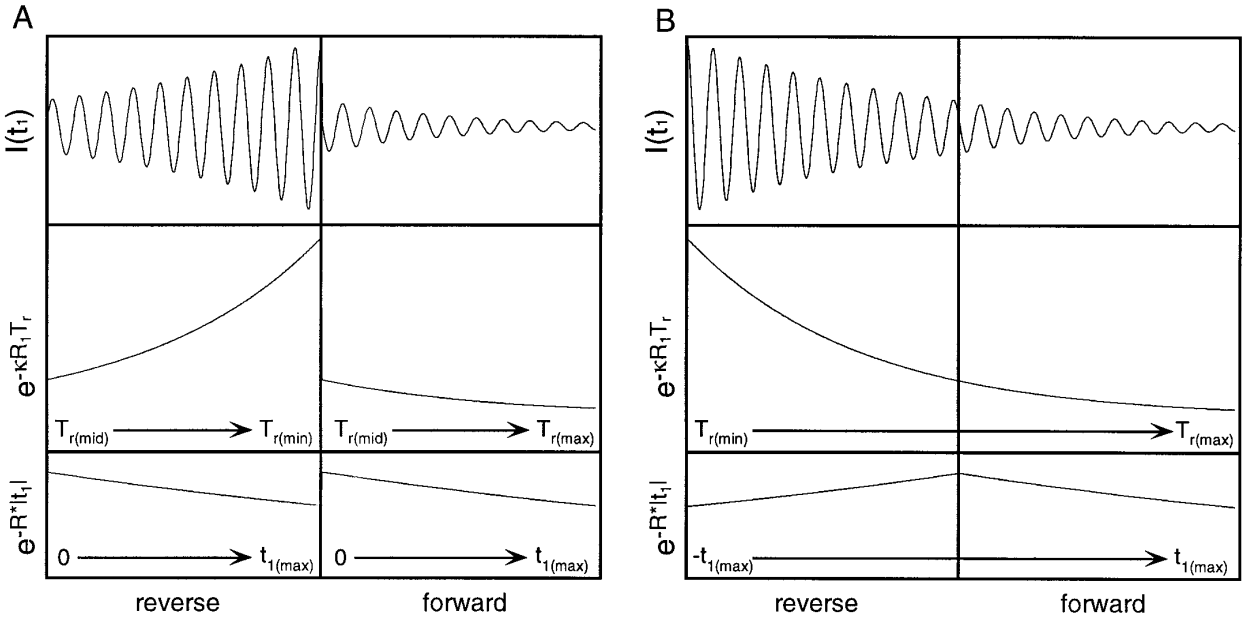

FIG. 1. Schematic of a negative-time accordion interferogram (A) reverse and forward components, as acquired; and (B) after time inversion and complex conjugation of the reverse component. Dependence of R_1 and R^* on relaxation terms T_r (middle) and t_1 (bottom) is indicated. The overall decay envelope of the interferogram (top) depends more heavily on R_1 than on R^*, as the scaled value of R_1 is typically much larger than R^* in constant time experiments.

t_3 (^{1}H) dimensions. T_r is covaried with t_1 as above to generate the forward and reverse components of a negative-time accordion experiment. As the 3D data set is conceptually similar to the HNCO experiment (*15*), this experiment will be referred to as the ^{13}CO R_1 HNCO accordion.

Figure 3 illustrates a different application of 3D accordion spectroscopy for the measurement of ^{15}N R_1 relaxation rates. The conventional experiment (Fig. 3A) is based on standard techniques (*1*). The new experiment in Fig. 3B will be referred to as the ^{15}N R_1 HNCO accordion. After the T_r accordion delay, magnetization is transferred from the amide ^{15}N spins to the ^{13}CO spins for frequency labeling and back to ^{15}N. This symmetric out-and-back transfer sequence is designed to employ as much of the constant-time transfer delay as possible for the acquisition of a maximum number of t_1 points. Thus, t_1 evolution occurs both before and after t_2 evolution, using a HMQC-style evolution period during t_2, in which both ^{15}N and ^{13}CO magnetization remain transverse. The flanking constant-time t_1 periods are adjusted to account for ^{15}N evolution during t_2. Thus, the transverse nitrogen operators evolve for a total of

$$-\frac{(T - t_1 + t_2)}{4} + \frac{(T + t_1 - t_2)}{4} + \frac{t_2}{2} - \frac{t_2}{2} + \frac{(T + t_1 - t_2)}{4} - \frac{(T - t_1 + t_2)}{4} = t_1. \qquad [10]$$

The ^{13}CO coherence is transverse for a total duration of t_2. The ^{15}N– ^{13}CO scalar coupling evolves for $T/2 = 1/(2J_{NCO})$ both before and after t_2.

EXPERIMENTAL

NMR spectra were obtained at 11.7 T and 300 K on a Bruker AMX-500 spectrometer equipped with a triple-resonance three-axis gradient probehead. The sample employed for all experiments was the third type III fibronectin domain of human tenascin (TNfn3), >99% ^{15}N/^{13}C enriched, at a concentration of 1.0 mM in 90%/10% H_2O/D_2O, pH 5.5 (unadjusted reading). ^{15}N R_1 relaxation measurements acquired via the conventional method were performed previously (*5*) on a ^{15}N-labeled sample on TNfn3. Spectral processing and extraction of t_1 interferograms was performed in Felix 2.3 (MSI) and NMRPipe (*3*).

The conventional ^{13}CO R_1 experiment was recorded as a series of six 2D data sets. Spectral widths of 1562.5 × 7812.5 Hz were used for the $t_1 \times t_2$ (^{15}N × ^{1}H) dimensions, recording 40 × 4096 complex points, with the ^{1}H carrier set to the H_2O frequency (4.73 ppm) and the ^{15}N carrier set at 119.5 ppm. Carrier frequencies for ^{13}CO and $^{13}C^{\alpha}$ pulses were 174.1 and 54.8 ppm, respectively. A total of 128 transients were recorded per t_1 increment. The parametric relaxation delays for the six datasets were 0.001 (repeated), 0.023, 0.50, 0.85, 1.30, and 2.00 s. Total acquisition time for these data sets was 24 h. PEP sensitivity enhancement in the ^{15}N dimension was performed using an in-house FORTRAN program. Spectral processing was performed in both

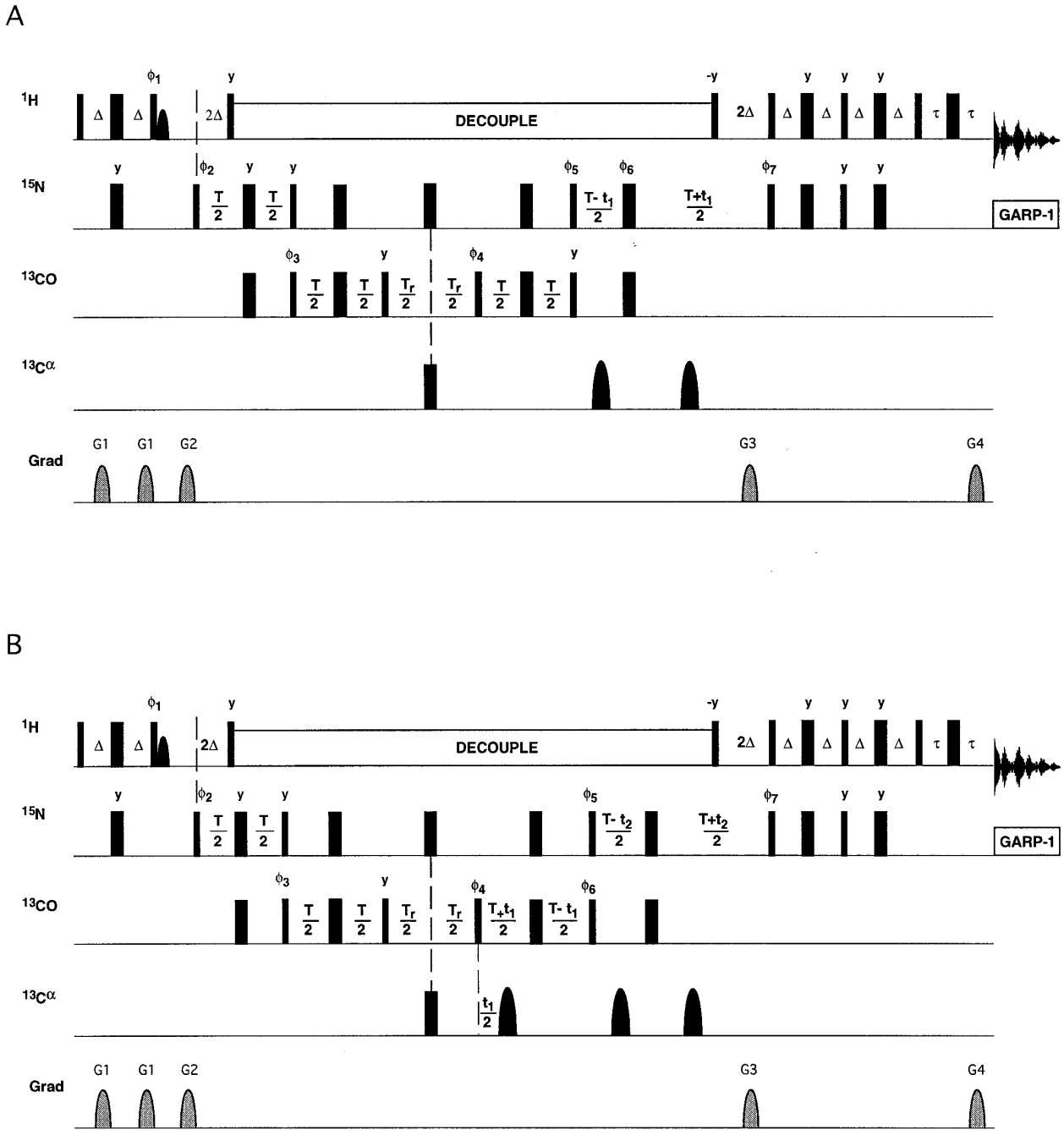

FIG. 2. Pulse sequences for (A) conventional 2D and (B) 3D HNCO accordion experiments for measuring ^{13}CO spin–lattice relaxation rate constants. Narrow and thick bars represent 90° and 180° pulses, respectively. Shaped $^{13}C^{\alpha}$ pulses are indicated by rounded bars. The rounded bar immediately following the 90° ^{1}H pulse with phase ϕ_1 is a water flip-back pulse (*29, 30*). Pulses were applied with x phase unless otherwise indicated. $\Delta = 1/(2J_{NH})$, $T \approx 1/(2J_{NCO})$, t_1 and t_2 are the incremented delays, T_r is the variable relaxation delay, and τ is greater than the length of gradient G4. In (A), T_r is varied between two-dimensional experiments. In (B) T_r is varied synchronously with the t_1 incrementable delay, such that $\kappa = \Delta T_r/\Delta t_1$. The WALTZ-16 sequence (*31*) with a field strength of 2.33 kHz was used to decouple the ^{1}H spins. The GARP-1 sequence (*32*) with a field strength of 0.52 kHz was used to decouple ^{15}N during acquisition. The phase cycling was as follows: (A) $\phi_1 = 2(y), 2(-y)$; $\phi_2 = 4(y), 4(-y)$; $\phi_3 = x, -x$; $\phi_4 = 16(x), 16(-x)$; $\phi_5 = x$; $\phi_6 = 8(x), 8(y), 8(-x), 8(-y)$; $\phi_7 = x$; receiver $= x, 2(-x), x, -x, 2(x), -x, 2[-x, 2(x), -x, x, 2(-x), x], x, 2(-x), x, -x, 2(x), -x$; and (*B*) $\phi_1 = 2(y), 2(-y)$; $\phi_2 = 4(y), 4(-y)$; $\phi_3 = x, -x$; $\phi_4 = x$; $\phi_5 = x$; $\phi_6 = 52°$; receiver $= x, 2(-x), x, -x, 2(x), -x$. In (A) frequency discrimination in t_1 was achieved using the PEP sensitivity-enhanced gradient method (*23*). In (B) frequency discrimination in t_1 was achieved using States–TPPI phase cycling (*33*) of ϕ_4 along with the receiver phase. Frequency discrimination in t_2 was achieved using the PEP sensitivity-enhanced gradient method (*23*). The N- and P-type signals were collected separately by inverting the sign of the G4 gradient pulse along with inversion of ϕ_7 in (*A*) and in (*B*). Axial peaks were shifted to the edge of the spectrum by inverting ϕ_5 and the receiver for each increment. All gradient pulses were sinusoidally shaped *xyz* gradient pulses: The durations and maximum amplitudes were as follows: G1 = 0.5 ms with $g_x = g_y = 0$ G/cm and $g_z = 8.0$ G/cm; G2 = 3.0 ms with $g_x = g_y = 0$ G/cm and $g_z = 15.0$ G/cm; G3 = 2.5 ms with $g_x = g_y = g_z = 20.0$ G/cm; G4 = 0.5 ms with $g_x = g_y = g_z = 10.1$ G/cm.

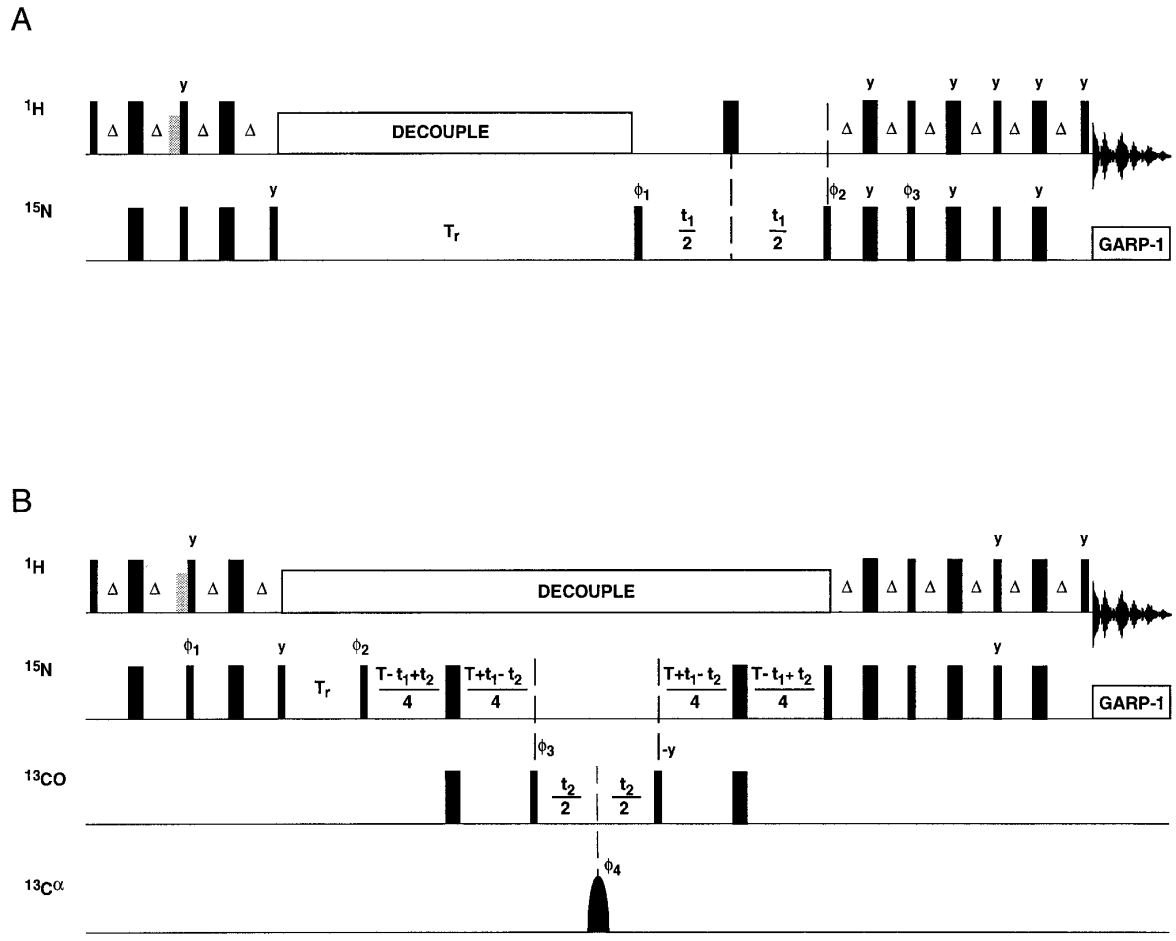

FIG. 3. Pulse sequences for (A) conventional 2D and (B) 3D HNCO accordion experiments for measuring ^{15}N spin–lattice relaxation rate constants. Narrow and thick bars represent 90° and 180° pulses, respectively. Shaped $^{13}C^{\alpha}$ pulses are indicated by rounded bars. The gray bars represents spin-lock purges pulse applied to the solvent resonance (*34*). Weak presaturation of the solvent resonance was employed prior to the first pulse shown in (B). The WALTZ-16 sequence (*31*) with a field strength of 2.33 kHz was used to decouple the ^{1}H spins. The GARP-1 sequence (*32*) with a field strength of 0.52 kHz was used to decouple ^{15}N during acquisition. $\Delta = 1/(2J_{NH})$, $T \approx 1/(J_{NCO})$, t_1 and t_2 are the incremented delays, and T_r is the variable relaxation delay. Pulses were applied with x phase unless otherwise indicated. Phase cycling was as follows: (A) $\phi_1 = x, -x, x, -x, -x, x, -x, x$; $\phi_2 = y$; $\phi_3 = 2(y), 2(-y)$; receiver $= x, -x, -x, x, -x, x, x, -x$; and (B) $\phi_1 = x, -x$; $\phi_2 = x$; $\phi_3 = 2(y), 2(-y)$; $\phi_4 = x, -x$; receiver $= x, -x, -x, x$. In (A) frequency discrimination in t_1 was achieved using a modified PEP scheme in which ϕ_2 was inverted on alternate t_1 experiments. In (B) frequency discrimination in t_1 was achieved using the PEP-Z sensitivity-enhancement method (*35*). Frequency discrimination in t_2 of (B) was achieved using States–TPPI phase cycling (*33*) of ϕ_3 along with the receiver phase.

t_1 and t_2 by applying a cosine bell apodization function and zero filling by a factor of two. Peak intensities and signal-to-noise were measured using NMRDraw (the graphical interface of NMRPipe). Decay curves were fitted to monoexponential equations using Kaleidagraph (Abelbeck Software).

The ^{13}CO R_1 HNCO accordion was recorded as a single 3D data set containing both the forward and reverse components of the negative-time accordion. Spectral widths of 1358.3 × 1562.5 × 7812.5 Hz were used in the $t_1 \times t_2 \times t_3$ (^{13}CO × ^{15}N × ^{1}H) dimensions, acquiring 80 × 32 × 1024 complex points (including the forward and reverse components). Carrier frequencies for each nucleus were as above. Thirty-two transients were collected for each t_1 increment. Total acquisition time for this data set was 62 h. The maximal value of T_r was set to 0.94 s, with $\Delta T_r = 11.78$ ms, corresponding to a value of $\kappa = 32$. Fourier transformation in t_3 (acquisition dimension) was performed by applying a squared cosine bell apodization function, zero filling by a factor of two, and multiplying the first complex point of every 1D vector by 0.5. Fourier transformation in t_2 (^{15}N dimension) was performed by applying a cosine bell apodization function and zero filling by a factor of two. Forward and reverse t_1 interferograms were not Fourier transformed, but were combined as outlined above for the negative-time accordion experiment. Signal-to noise (S/N) was estimated as the standard deviation of t_1 interferograms containing noise only. In-house

FORTRAN routines were then used to identify frequency components with the HSVD algorithm (*24*) and to apply Levenberg–Marquardt nonlinear least-squares fitting (*25*) to determine the decay constants of interest.

The results of the conventional ^{15}N R_1 experiment applied to TNfn3 have been reported elsewhere (*5*). Spectral widths of 1517.5 × 12500 Hz were used for the $t_1 \times t_2$ (^{15}N × ^{1}H) dimensions, recording 128 × 8192 complex points, with the ^{1}H and ^{15}N carrier frequencies as above. Thirty-two transients were recorded per t_1 increment. The parametric relaxation delays for the 13 2D data sets were as follows: 0.02, 0.07 (repeated), 0.16, 0.28 (repeated), 0.42, 0.60 (repeated), 0.95, 1.80 (repeated), and 2.00 s. Total acquisition time for these data sets was 49 h. Several different resolution enhancement schemes were applied to the spectra in order to resolve partially overlapped peaks in the t_1 and/or t_2 dimensions (*5*). Peak intensities were measured using Felix 2.3 (MSI). Uncertainties and nonlinear least-squares fits of R_1 values were determined as described previously (*26*).

The ^{15}N R_1 HNCO accordion was recorded as a single 3D data set containing both the forward and reverse components of the negative-time accordion. Spectral widths of 1623.4 × 1358.3 × 7812.5 Hz were used in the $t_1 \times t_2 \times t_3$ (^{15}N × ^{13}CO × ^{1}H) dimensions, acquiring 192 × 32 × 1024 complex points (including the forward and reverse components). Carrier frequencies for each nucleus were as above. Sixteen transients were collected for each t_1 increment stored. Total acquisition time for this data set was 72 h. The maximal value of T_r was set to 1.01 s, with ΔT_r = 5.24 ms, corresponding to a value of κ = 8.5. Fourier transformation in t_3 (acquisition dimension) was performed subsequent to use of a digital low-pass filter to suppress solvent signal (*27*), scaling of the first point by a factor of two (*28*), apodization with an exponential decay function with a decay constant of 7 Hz, and zero-filling by a factor of two. Fourier transformation in t_2 (^{13}CO dimension) was performed after apodization with a Kaiser function ($\theta = \pi$) and zero-filling by a factor of two. Forward and reverse t_1 interferograms were not Fourier transformed, but were combined as outlined above for a negative-time accordion. The resultant t_1 interferograms encoding both ^{15}N evolution and ^{15}N R_1 relaxation were extracted and analyzed as above.

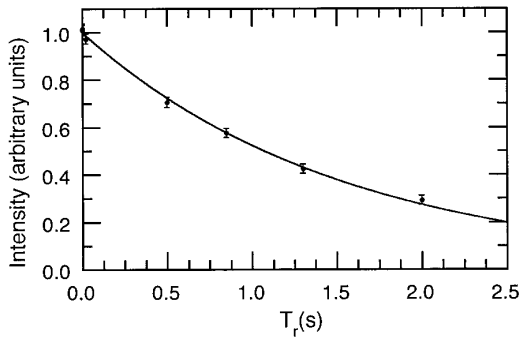

FIG. 4. Conventional ^{13}CO R_1 relaxation decay curve for residue Ser58, acquired with the experiment described in the legend to Fig. 2A.

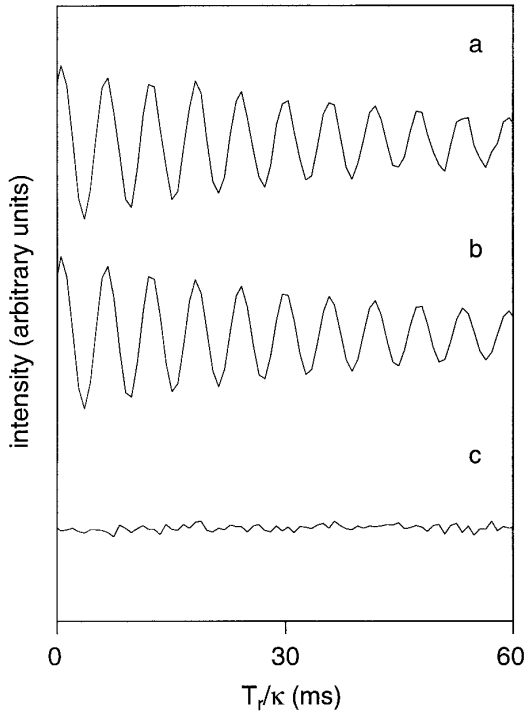

FIG. 5. Typical ^{13}CO R_1 negative-time accordion interferogram for residue Ser58, acquired using the experiment detailed in the legend to Fig. 2B. (a) Acquired data, after inversion and complex conjugation of the reverse component; (b) interferogram simulated from curve fitting to a single frequency; (c) residual differences between (a) and (b).

RESULTS AND DISCUSSION

Constant-time negative accordion experiments were performed to measure ^{13}CO and ^{15}N R_1 relaxation in TNfn3. Conventional ^{13}CO R_1 measurements were performed for comparison; ^{15}N R_1 measurements reported earlier for a sample of ^{15}N-labeled TNfn3 (*5*) were also used for comparison.

An example of a typical ^{13}CO relaxation decay curve acquired by conventional methods is shown in Fig. 4. A decaying interferogram from the corresponding 3D accordion experiment is shown in Fig. 5. Table 1 compares R_1 values for 20 residues of TNfn3 determined by both of these methods. The differences between the two experiments were evaluated using a pairwise Z score for each residue:

$$Z = \frac{R_1^{\mathrm{acc}} - R_1^{\mathrm{conv}}}{\sqrt{\sigma_{\mathrm{acc}}^2 + \sigma_{\mathrm{conv}}^2}}, \qquad [11]$$

in which R_1^{acc} and R_1^{conv} are the fitted rate constants and σ_{acc} and σ_{conv} are the uncertainties for the accordian and conventional experiments, respectively.

TABLE 1
Selected ^{13}CO R_1 Relaxation Rate Constants for TNfn3

Residue	R_1 conventional (s^{-1})	R_1 accordion (s^{-1})
Ala-5	0.692 ± 0.023	0.693 ± 0.019
Ala-27	0.743 ± 0.011	0.736 ± 0.031
Ile-29	0.740 ± 0.035	0.730 ± 0.035
Asp-30	0.747 ± 0.032	0.658 ± 0.026
Ile-32	0.726 ± 0.032	0.730 ± 0.033
Leu-34	0.674 ± 0.026	0.707 ± 0.023
Gly-43	0.640 ± 0.015	0.682 ± 0.016
Thr-47	0.719 ± 0.034	0.708 ± 0.022
Asn-55	0.710 ± 0.021	0.691 ± 0.024
Ser-58	0.649 ± 0.023	0.631 ± 0.096
Ile-59	0.705 ± 0.043	0.676 ± 0.039
Pro-64	0.752 ± 0.019	0.734 ± 0.033
Thr-66	0.744 ± 0.031	0.737 ± 0.032
Glu-67	0.745 ± 0.061	0.707 ± 0.053
Glu-69	0.692 ± 0.028	0.727 ± 0.027
Arg-76	0.691 ± 0.027	0.746 ± 0.024
Met-79	0.664 ± 0.026	0.671 ± 0.021
Lys-85	0.731 ± 0.023	0.702 ± 0.022
Glu-86	0.657 ± 0.034	0.716 ± 0.042
Phe-88	0.708 ± 0.020	0.694 ± 0.029

The average of Z scores is expected to be close to zero if both experiments accurately measure the true value of R_1 (or if they are both biased in the same sense). The variance of the Z scores is expected to be close to unity if the distribution of differences approximates a normal distribution. With an average Z score of -0.009 and variance of 0.84, the differences between the two ^{13}CO experiments can be considered essentially random. The accuracy of the experiments can also be assessed by comparing the average uncertainties of the R_1 values determined. Weighted mean uncertainties of these experiments are similar: 0.023 s^{-1} (conventional) and 0.026 s^{-1} (accordion), implying similar degrees of precision. The ^{13}CO accordion required slightly more than twice the acquisition time to achieve similar precision; however, this is not unexpected, because phase cycling for frequency discrimination in the t_1 (^{13}CO) dimension can retain only one of two orthogonal signal components.

The ^{15}N 3D accordion HNCO experiment was used to determine ^{15}N R_1 values for 74 residues from TNfn3, which were compared to values obtained previously (*5*). An interferogram for the 3D accordion experiment is shown in Fig. 6. Z scores were calculated as for the ^{13}CO experiments above to give an average of 0.23 and a variance of 1.5. The accordion ^{15}N R_1 values measured in the ^{13}C/^{15}N-labeled protein are larger by 1.2% than for the ^{15}N-labeled protein. The difference is the result of additional relaxation caused by the ^{13}CO and $^{13}C^{\alpha}$ nuclei in the double-labeled protein. The relaxation contributions from ^{13}CO and $^{13}C^{\alpha}$ are approximately given by

$$R_1^{NC}/R_1^{NH} = \frac{\gamma_C^2}{\gamma_H^2}\left(\frac{r_{NH}}{r_{NC}}\right)^6\left(1 + \frac{2\gamma_N^2}{(\gamma_N + \gamma_C)^2}\right) \quad [12]$$

using r_{NH} = 1.02 Å, r_{NCO} = 1.33 Å, $r_{NC\alpha}$ = 1.45 Å, $\gamma_C = 6.728 \times 10^7$ $T^{-1}s^{-1}$, $\gamma_N = -2.71 \times 10^{-7}$ T^{-1} s^{-1} and $\gamma_H = 2.6752 \times 10^8$ $T^{-1}s^{-1}$. Using Eq. [12], the relative contribution to R_1 from ^{13}CO and $^{13}C^{\alpha}$ is calculated to be 4%, slightly larger than the experimental result.

The 3D ^{15}N R_1 HNCO accordion experiment, unlike the conventional 2D ^{15}N R_1 experiment, is subject to relaxation losses incurred during T when magnetization is transferred to and from the ^{13}CO nucleus. As a result, the weighted mean uncertainties were 0.079 s^{-1} for the accordion experiment, compared to 0.022 s^{-1} for the conventional experiment, even though the accordion acquisition time was somewhat longer. In addition, some residues undergoing chemical exchange yielded S/N values too low to permit quantification. However, all resonances were clearly resolved in the 3D accordion experiment, whereas accurate R_1 values for resonances that were partially overlapped in the conventional data set could only be determined by applying strong resolution enhancement techniques (*2, 5*). For these residues, weighted mean uncertainties were increased to 0.112 s^{-1}, and significantly better precision was obtained in the 3D accordion experiment.

CONCLUSION

A new method has been developed for the measurement of relaxation rate constants for molecules with poorly resolved

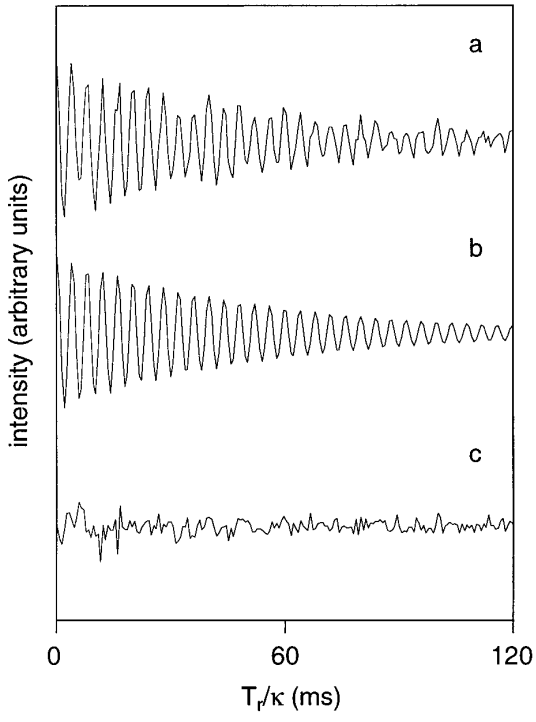

FIG. 6. Typical ^{15}N R_1 negative-time accordion interferogram for residue Ser58, acquired using the experiment detailed in Fig. 3B. (a) Acquired data, after inversion and complex conjugation of the reverse component; (b) interferogram simulated from curve fitting to a single frequency; (c) residual differences between (a) and (b).

NMR spectra. This method combines elements from conventional approaches, employing triple-resonance techniques to provide additional spectral resolution. Accordion spectroscopy is employed to limit acquisition to a single three-dimensional data set.

Measurement of ^{13}CO R_1 relaxation rates by this new method has been shown to retain similar precision while providing improved resolution compared to conventional 2D methods. Thus, the 3D ^{13}CO accordion experiment is generally preferable to the conventional 2D approach. The improved resolution of the 3D ^{15}N R_1 accordion experiment is obtained at some cost in sensitivity for well-resolved resonances, because transfer of magnetization to and from ^{13}CO nuclei incurs relaxation losses not present in the conventional 2D methods. Therefore, the 3D ^{15}N accordion experiment is most useful for resonances that are overlapped in 2D spectra.

In these experiments, relaxation delays have been covaried with evolution periods corresponding to like nuclei, i.e., ^{15}N R_1 relaxation covaried with ^{15}N t_1 evolution. There is no requirement, however, that this be the case. For example, a ^{15}N relaxation delay could be covaried with a ^{13}CO evolution period if this proved advantageous for resolution. Also, an accordion experiment need not employ a constant-time evolution period, although it proves most efficient in the above experiments, because constant-time evolution occurs during a requisite magnetization transfer step. Thus no additional relaxation losses are incurred in these cases. In principle, two independent accordion experiments could be combined in one 3D experiment encoding independent relaxation delays in both t_1 and t_2 indirect periods.

For NMR studies of dynamics, sets of three relaxation parameters are often measured: R_1, R_2, or $R_{1\rho}$, and heteronuclear NOE (*1*). Here we have presented applications for the measurement of R_1 values; however, the same principles can be extended to $R_{1\rho}$ measurements. NOE values are typically determined from the ratio of two 2D correlation spectra, acquired with and without presaturation of the indirect nucleus. Conversion of these experiments to 3D HNCO-type experiments is straightforward. As the conventional 2D NOE experiments already require averaging a large number of transients, 3D versions of these experiments need not dramatically increase acquisition times.

The new 3D accordion methods should be of use to spectroscopists studying relaxation and dynamics in large macromolecules, particularly in cases where limited spectral resolution would otherwise make accurate relaxation measurements difficult or impossible. The experiments described here for measuring relaxation of ^{13}CO and ^{15}N spins should be extensible to $^{13}C^{\alpha}$ and other nuclear spins.

ACKNOWLEDGMENTS

The authors thank Gina Briscoe and Harold Erickson (Duke University Medical Center) for providing the $^{15}N/^{13}C$-enriched tenascin TNfn3 and Nathan Astrof and Clay Bracken (Columbia University) for helpful discussions. This work was supported by grants to A.G.P. from the National Institute of Health (GM-50291) and a Beckman Young Investigator Award.

REFERENCES

1. A. G. Palmer, J. Williams, and A. McDermott, Nuclear magnetic resonance studies of biopolymer dynamics, *J. Phys. Chem.* **100,** 13,293–13,310 (1996).
2. N. J. Skelton, A. G. Palmer, M. Akke, J. Kördel, M. Rance, and W. J. Chazin, Practical aspects of two-dimensional proton-detected ^{15}N spin relaxation measurements, *J. Magn. Reson. B* **102,** 253–264 (1993).
3. F. Delaglio, S. Grzesiek, G. Vuister, G. Zhu, J. Pfeifer, and A. Bax, NMRPipe: A multidimensional spectral processing system based on UNIX pipes, *J. Biomol. NMR* **6,** 277–293 (1995).
4. P. Mishra, Z. Zolnai, N. Juranic, and S. Macura, Measurement of relaxation rates from 2D spectra with partial overlap, *J. Magn. Reson.* **125,** 358–363 (1997).
5. P. A. Carr, H. P. Erickson, and A. G. Palmer, Backbone dynamics of homologous fibronectin type III cell adhesion domains from fibronectin and tenascin, *Structure* **5,** 949–959 (1997).
6. A. M. Mandel, M. Akke, and A. G. Palmer, Dynamics of ribonuclease H: Temperature dependence of motions on multiple time scales, *Biochemistry* **35,** 16,009–16,023 (1996).
7. J. Cavanagh, W. J. Fairbrother, A. G. Palmer, and N. J. Skelton, ''Protein NMR Spectroscopy: Principles and Practice,'' Academic Press, San Diego (1996).
8. G. Bodenhausen, and R. R. Ernst, The accordion experiment, a simple approach to three-dimensional NMR Spectroscopy, *J. Magn. Reson.* **45,** 367–373 (1981).
9. G. Bodenhausen, and R. R. Ernst, Direct determination of rate constants of slow dynamic processes by two-dimensional ''accordion'' spectroscopy in nuclear magnetic resonance, *J. Am. Chem. Soc.* **104,** 1304–1309 (1982).
10. J. R. Tolman and J. H. Prestegard, Measurement of amide ^{15}N–^{1}H one-bond couplings in proteins using accordion heteronuclear-shift-correlation experiments, *J. Magn. Reson. B* **112,** 269–274 (1996).
11. G. Kontaxis and J. Keeler, The accordion approach for ''taylored'' TOCSY, *J. Magn. Reson. A* **115,** 35–41 (1995).
12. A. M. Mandel and A. G. Palmer, Measurement of relaxation-rate constants using constant-time accordion NMR spectroscopy, *J. Magn. Reson. A* **110,** 62–72 (1994).
13. L. E. Kay and J. H. Prestegard, Spin–lattice relaxation rates of coupled spins from 2D accordion spectroscopy, *J. Magn. Reson.* **77,** 599–605 (1988).
14. T. Szyperski, G. Wider, J. H. Bushweller, and K. Wüthrich, Reduced dimensionality in triple-resonance NMR experiments, *J. Am. Chem. Soc.* **115,** 9307–9310 (1993).
15. L. E. Kay, M. Ikura, R. Tschudin, and A. Bax, Three-dimensional triple-resonance NMR spectroscopy of isotopically enriched proteins, *J. Magn. Reson.* **89,** 496–514 (1990).
16. L. Zeng, M. W. F. Fischer, and E. R. P. Zuiderweg, Study of protein dynamics in solution by measurement of $^{13}C^{\alpha}$–^{13}CO NOE and ^{13}CO longitudinal relaxation, *J. Biomol. NMR* **7,** 157–162 (1996).
17. K. T. Dayie and G. Wagner, Carbonyl carbon probe of local mobility in ^{13}C, ^{15}N-enriched proteins using high-resolution nuclear magnetic resonance, *J. Am. Chem. Soc.* **119,** 7797–7806 (1997).
18. V. Sklenar, D. Torchia, and A. Bax, Measurement of carbon-13

longitudinal relaxation using ^{1}H detection, *J. Magn. Reson.* **73,** 375–379 (1987).

19. D. J. States, R. A. Haberkorn, and D. J. Ruben, A two-dimensional nuclear Overhauser experiment with the pure absorption phase in four quadrants, *J. Magn. Reson.* **48,** 286–292 (1982).

20. A. G. Palmer, J. Cavanagh, P. E. Wright, and M. Rance, Sensitivity improvement in proton-detected two-dimensional heteronuclear correlation NMR spectroscopy, *J. Magn. Reson.* **93,** 151–170 (1991).

21. G. Zhu and A. Bax, Improved linear prediction for truncated signals of known phase, *J. Magn. Reson.* **90,** 405–410 (1990).

22. A. Bax, M. Ikura, L. E. Kay, and G. Zhu, Removal of F1 baseline distortion and optimization of folding in multidimensional NMR spectra, *J. Magn. Reson.* **91,** 174–178 (1991).

23. L. E. Kay, P. Keifer, and T. Saarinen, Pure absorption gradient enhanced heteronuclear single quantum correlation spectroscopy with improved sensitivity, *J. Am. Chem. Soc.* **114,** 10,663–10,665 (1992).

24. H. Barkhuijsen, R. de Beer, and D. van Ormondt, Improved algorithm for noniterative time-domain model fitting to exponentially damped magnetic resonance signals, *J. Magn. Reson.* **73,** 553–557 (1987).

25. W. H. Press, B. P. Flannery, S. A. Teukolsky, and W. T. Vetterling, ''Numerical Recipes: The Art of Scientific Computing,'' 2nd. ed., Cambridge Univ. Press, Cambridge (1986).

26. A. G. Palmer, M. Rance, and P. E. Wright, Intramolecular motions of a zinc finger DNA-binding domain from xfin characterized by proton-detected natural abundance ^{13}C heteronuclear NMR spectroscopy, *J. Am. Chem. Soc.* **113,** 4371–4380 (1991).

27. D. Marion, M. Ikura, and A. Bax, Improved solvent suppression in one- and two-dimensional NMR spectra by convolution of time-domain data, *J. Magn. Reson.* **84,** 425–430 (1989).

28. G. Otting, H. Widmer, G. Wagner, and K. Wüthrich, Origin of t_1 and t_2 ridges in 2D NMR spectra and procedures for suppression, *J. Magn. Reson.* **66,** 187–193 (1986).

29. S. Grzesiek and A. Bax, The importance of not saturating H_2O in protein NMR. Application to sensitivity enhancement and NOE experiments, *J. Am. Chem. Soc.* **115,** 12,593–12,594 (1993).

30. L. E. Kay, G.-Y. Xu, and T. Yamazaki, Enhanced-sensitivity triple-resonance spectroscopy with minimal H_2O saturation, *J. Magn. Reson. A* **109,** 129–133 (1994).

31. A. J. Shaka, J. Keeler, T. Frenkiel, and R. Freeman, An improved sequence for broadband decoupling: WALTZ-16, *J. Magn. Reson.* **52,** 334–338 (1983).

32. A. J. Shaka, P. B. Barker, and R. Freeman, Computer-optimized decoupling scheme for wideband applications and low-level operation, *J. Magn. Reson.* **64,** 547–552 (1985).

33. D. Marion, M. Ikura, R. Tschudin, and A. Bax, Rapid recording of 2D NMR spectra without phase cycling. Application to the study of hydrogen exchange in proteins, *J. Magn. Reson.* **85,** 393–399 (1989).

34. B. A. Messerle, G. Wider, G. Otting, C. Weber, and K. Wüthrich, Solvent suppression using a spin lock in 2D and 3D NMR spectroscopy with H_2O solutions, *J. Magn. Reson.* **85,** 608–613 (1989).

35. M. Akke, P. A. Carr, and A. G. Palmer, Heteronuclear-correlation NMR spectroscopy with simultaneous isotope filtration, quadrature detection, and sensitivity enhancement using z rotations, *J. Magn. Reson. B* **104,** 298–302 (1994).